Hindawi
Mathematical Problems in Engineering
Volume 2021, Article ID 5527073, 11 pages
https://doi.org/10.1155/2021/5527073

Research Article

Analysis of the Mechanical Characteristics of Different Track Bed Types in Heavy-Haul Railway Tunnels

Ziqiang Li,[1,2] **Weiwei Huang**,[1] **Zhifan Xu**,[1] **Xiao Tang**,[1] **Mingnian Wang**,[3] **Li Yu**,[3] **and Zheng Li**[2]

[1]*School of Civil Engineering and Architecture, Chongqing University of Science & Technology, Chongqing, China*
[2]*Key Laboratory of New Technology for Construction of Cities in Mountain Area, Ministry of Education, Chongqing University, Chongqing 400045, China*
[3]*Key Laboratory of Transportation Tunnel Engineering, Ministry of Education, Southwest Jiaotong University, Chengdu, China*

Correspondence should be addressed to Ziqiang Li; lzq1102dd@163.com

Received 25 January 2021; Revised 7 May 2021; Accepted 15 May 2021; Published 24 May 2021

Academic Editor: Isabella Torcicollo

Based on field measurement data from the Fuyingzi Tunnel and Hongshila Tunnel on the Zhangtang Railway, a comparative analysis was conducted on the characteristics of a ballast bed and ballastless slab track, which are commonly used in the track structures of heavy-haul railway tunnels. According to the relevant domestic standards and the theory of the stress diffusion angle, a wheel-rail sharing ratio and theoretical calculation method for the added value of the trainload on the surface and bottom of different track bed types was proposed. In accordance with the measured data, the dynamic load thresholds and distributions on the surface and bottom of different track bed types were analysed and compared with the theoretical results. The results show that the theoretical equation has high accuracy and good applicability. The ballast bed can better cushion the heavy loads, while the ballastless slab track is better able to accomplish train load attenuation. In addition, the distribution on the bottom of the ballastless slab track is "triangular", while the distribution at the surface or bottom of the ballastless track and ballast bed is "saddle-shaped." The ballast bed is subjected to a greater load from the vehicle, and the long-term effect is more pronounced. These results can provide a theoretical basis for the stress analysis and design parameters of heavy-haul railway tunnel track beds.

1. Introduction

Presently, heavy-haul railways have become the main focus of development for freight transportation in various countries [1, 2]. Because heavy-haul railways have the characteristics of large heavy axles, large gross weights, high vehicle density, and large rail transport of traffic, the basement structure of a heavy-haul railway tunnel will bear a greater train dynamic load than ordinary railway tunnels [3, 4]. The track bed is most significantly affected by the dynamic loads from trains during the operation of heavy-haul railway tunnels [5]. The mechanical behaviour of a ballastless slab track is relatively clear, and it can provide high ride comfort with less maintenance; however, problems of loud noise and severe vibration are caused by the integrated structure and rigid nature of a ballastless slab track. In contrast, the construction period and cost of ballast beds are easy to control, and the train load transfer range is small; however, the mechanical characteristics of ballast beds are complex. Ballast beds and ballastless slab tracks remain the two main types of track bed used in China, and they are also the main types of track bed used in heavy-haul railway tunnels. Maintaining a good service status of the track bed is critical for ensuring railway smoothness and providing a stable running interface for the train operation [6, 7]. The high ride comfort of the rail surface can provide a stable running interface for the train operation. It is of great importance to analyse the dynamic loading of heavy-haul

trains on ballast beds and ballastless slab tracks to investigate the mechanical properties of the track bed. This is also the premise for determining reasonable design parameters for the track bed and ensuring the operational safety of heavy-haul railway tunnels.

Some domestic and foreign studies have been conducted on the mechanical characteristics of ballast beds and ballastless slab tracks. Ganzalez-Nicieza et al. [8] determined that sleepers at the loading positions of heavy-haul trains are the main stress components, and the load action is greatly reduced outside the range of 5 m, but the distribution of load is not clear. Yang et al. [9] analysed the influence of different track bed types on subgrade stress characteristics, a two-dimensional dynamic finite element model is established based on effective elastic stiffness, and the results show that when the train speed is greater than 10% of the Rayleigh wave velocity of the subgrade, the dynamic effect begins to appear. Sadeghi [10] measured the loads transferred from the rail to the sleeper and from the sleeper to the ballast as a function of the train speed and proposed ratios to calculate the dynamic impact factors and ballast–sleeper pressure distribution patterns for the design of sleepers, but there is no research on the ballastless track bed. Lazorenko et al. [11] concluded that the track foundation is the most important element in railway track construction, and the main factors that determine the dynamics of the soil behaviour of the railbed under cyclic loading from heavy-haul trains are the magnitude and duration of the loads. Based on the space–time-dependent characteristics and interaction between the vehicles, ballast bed, and subgrade, Xu and Cai [12] established a spatially coupled dynamic model to describe the dynamic transmission characteristics of a ballast track and subgrade. Yang et al. [13] simulated the effects of gradation and particle shape on the mechanical characteristics of a ballast bed using the discrete element method and found that a reasonable gradation could provide the ballast bed with good mechanical properties; the contact force between ballasts under this condition was distributed in a conical shape over 45°. The above research has mostly investigated the trainload transfer law for a single structural type of track bed, focusing largely on the subgrade; however, research on the mechanical characteristics of different heavy-haul railway tunnel track bed types under the same conditions (i.e., the same surrounding rock, train load, and section type) is very limited, and there is no research on the dynamic load calculation method of heavy-haul railway tunnel track bed.

In this study, a theoretical calculation method for the dynamic load on the surface and bottom of track beds in heavy-haul railway tunnels is proposed based on the relevant domestic regulations and previous research results. Through remote real-time data acquisition from a monitoring section of class III surrounding rock in the Fuyingzi Tunnel and Hongshila Tunnel on the Zhangtang Railway, the distribution and threshold of the dynamic load on the surface and bottom of different track bed types are obtained. As a result, the mechanical characteristics of different track bed types in a double-track heavy-haul railway tunnel can be determined, and the measured value can be compared to the theoretical calculation value. The results of this study can provide a reference for the analysis of mechanical properties and determination of design parameters for ballast beds and ballastless slab tracks in heavy-haul railway tunnels.

2. Theoretical Calculation Method

When the load from a heavy-haul train acts on the rail, it is transmitted downward from the surface of the track bed through sleepers. The contact pressure between a sleeper and the track bed is calculated based on the dynamic axle load and the contact area of the sleeper bottom. Then, based on the assumption of stress conservation, the load on the filling layer surface is calculated through the stress dispersion angle [14, 15].

2.1. Dynamic Loads on the Surface of Track Bed. In Li et al. [16], based on the method of force transfer of the sleeper, a pseudo-static method for the dynamic load on the sleeper bottom is proposed as given in equation (1)

$$\sigma = p\frac{(1+\alpha v)}{\mathrm{BL}}, \tag{1}$$

where P is the static axle load; α is the dynamic impact coefficient, also known as the speed influence coefficient, which has a value of 0.005 for common rail, 0.004 for continuously welded rails, and 0.003 for high-speed railways; v is the train speed, which is set to a value of 300 km/h even if the actual speed is greater than 300 km/h; B is the average width of the bottom surface of the sleeper, which often has a value of 0.314 m; and L is the length of the sleeper, which is 2.6 m.

Lv et al. [17] conducted laboratory experiments and numerical simulations to determine the pile efficacy of a longitudinal sleeper under a heavy-haul train load. The results showed that when the heavy-haul train axle load reached 300 kN, the sleeper pile efficacy below the position of the bogie was 33.4%. The results also showed that the pile efficacy of the corresponding position of the sleeper will increase with increasing heavy-haul train axle load. The coefficient value of 0.26 in the Code for Design on Subgrade of Railway in China [18] is obtained from experience with common rails and high-speed rails with an axle load that is not greater than 170 kN. Using the interpolation method, the pile efficacy of a 270 kN axle load can be estimated as approximately 0.32.

Given these facts, equation (1) was corrected and revised by introducing the load distribution coefficient, γ, to reduce the dynamic load under different axle loads. The more accurate calculation formula in equation (2) is thus obtained for the dynamic load of the sleeper bottom.

$$\sigma = \frac{\gamma p(1+\alpha v)}{\mathrm{BL}}, \tag{2}$$

where P is the static axle load, which is consistent with equation (1); α, v, B, and L are also the same as in equation (1); and γ is the load distribution coefficient, which is 0.32 for a 270 kN axle load and 0.33 for a 300 kN axle load.

2.2. Dynamic Loads on the Bottom of the Track Bed. In China, the stress transfer in the slab is divided into three layers, each with different calculations. The thickness of the track bed in China is generally 30–35 cm, which is calculated according to the second layer. Then, combined with the sleeper sharing ratio, the parameters are simplified, and the calculation of the bottom contact pressure for different types of ballast is proposed as shown in equation (3)

$$\sigma = \frac{\gamma P(1 + \alpha v)}{2BL \tan \varphi}, \tag{3}$$

where P is the motor wheel load; B and L are the same as in equation (2); φ is the stress diffusion angle calculated based on the internal friction angle, which is 45° for ballastless slab tracks and 35° for ballast beds; and γ is the load distribution coefficient, which is the same as in equation (2).

3. Remote Monitoring

Sangat and Indrawan-Santiago [19] noted that remote monitoring and sensor technology can be effectively used in heavy-haul railway tunnels. To ensure that the results are objective and accurate, two double-track tunnels were selected on the Zhangtang Railway, and actual train data was recorded by selecting appropriate monitoring sections and burying survey points.

3.1. General Project Information. The Zhangtang Railway is the third energy channel that has been built in China, and it mainly services freight transport. The length of the Fuyingzi Tunnel is 10023 m, and the type of track bed is a ballastless slab track. The length of the Hongshila Tunnel is 5815 m, and the type of track bed is a ballast bed. The Fuyingzi Tunnel has two tracks, with a freight line on the left and a passenger line on the right. The section shapes of the two tunnels are completely consistent, and the cross section under class III surrounding rock is shown in Figure 1.

According to the in situ direct shear test conducted by the Zhangtang Railway and the Railway Tunnel Design Code in China [18], the physical parameters of the class III surrounding rock and tunnel structure are summarised in Table 1.

3.2. Sensor Placement. The fibre grating pressure sensor shown in Figure 2 is used for site monitoring. Measuring points are embedded on the surface and bottom of the track bed and the surface of the invert filling. This pressure sensor has many advantages, such as strong anti-interference and long-term stability, and even selecting a large range does not affect its accuracy. More importantly, this sensor allows for the realisation of dynamic contact pressure acquisition and remote transmission.

The monitoring sections in Fuyingzi Tunnel are located under class III, IV, and V surrounding rock conditions, and the monitoring sections of Hongshila Tunnel are under class III surrounding rock. In both tunnels, only the left line is a heavy-haul line. The distribution of measuring points and the installation of sensors are shown in Figure 3.

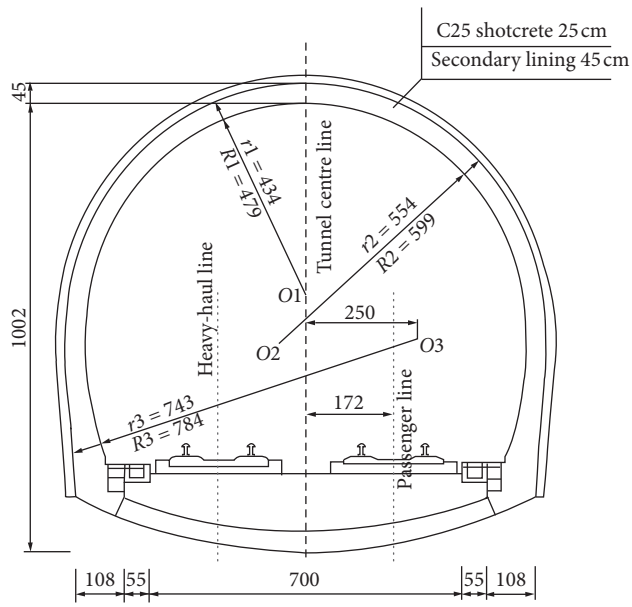

Figure 1: Cross section of the double-track heavy-haul railway tunnel under class III surrounding rock (units: cm).

The measurement range of the soil pressure gauges should consider that the tunnel structure is statically indeterminate, and the structural stress caused by the long-term loading is difficult to release. The measurement range of soil pressure gauges DT-1-DT-1 distributed on the track bed surface is 10 MPa, while that of pressure gauges DT-3-DT-5 on the track bed bottom is 5 MPa. Because the tunnel structure is a statically indeterminate structure, the long-term load will cause stress accumulation, so the selected sensor range is large but still applicable.

3.3. Remote Monitoring and Control System. First, sensors were installed at all of the measurement points on the track bed. Then, according to the measured wavelength, a sensor network is built (as shown in Figure 4); the main cable provides access to the communication rooms built at the tunnel entrance. Finally, a fibre grating demodulator, as shown in Figure 5, is used to realise remote data acquisition.

Currently, in the Fuyingzi Tunnel and Hongshila Tunnel of the Zhangtang Railway, the train axle load is 270 kN and the speed is 80 km/h. A monitoring system is set up to trigger an alarm and collect data only when trains have just passed the measurement sections to save computer storage space.

4. Analysis of Dynamic Data

According to the calculation of the sensor wavelength collected remotely in Fuyingzi Tunnel and Hongshilao Tunnel of the Zhangtang Railway, the dynamic load distributions on the surface and bottom of different types of track bed are basically similar. Owing to the length limitations, one heavy-haul train under the same conditions as the class III surrounding rock is first taken as an example, and the typical dynamic load time-history curves of the

Table 1: Structural parameters and class III surrounding rock parameters on the Zhangtang Railway.

Structure	Elastic modulus (GPa)	Poisson's ratio	Severe (kN·m^{-3})	Cohesion (MPa)	Friction (°)
Surrounding rock	13.0	0.24	24.0	0.012	38
Primary support	28.0	0.20	23.0	—	—
Secondary lining	31.0	0.20	23.0	—	—
Inverted arch filling	28.5	0.20	23.0	—	—
Inverted arch	31.0	0.20	23.0	—	—
Ballastless slab track	33.5	0.20	25.0	—	—
Ballast bed	—	0.25	18.5	—	—

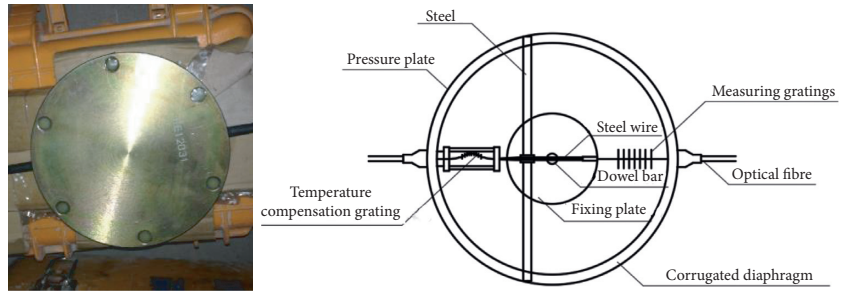

Figure 2: Fibre grating pressure sensor.

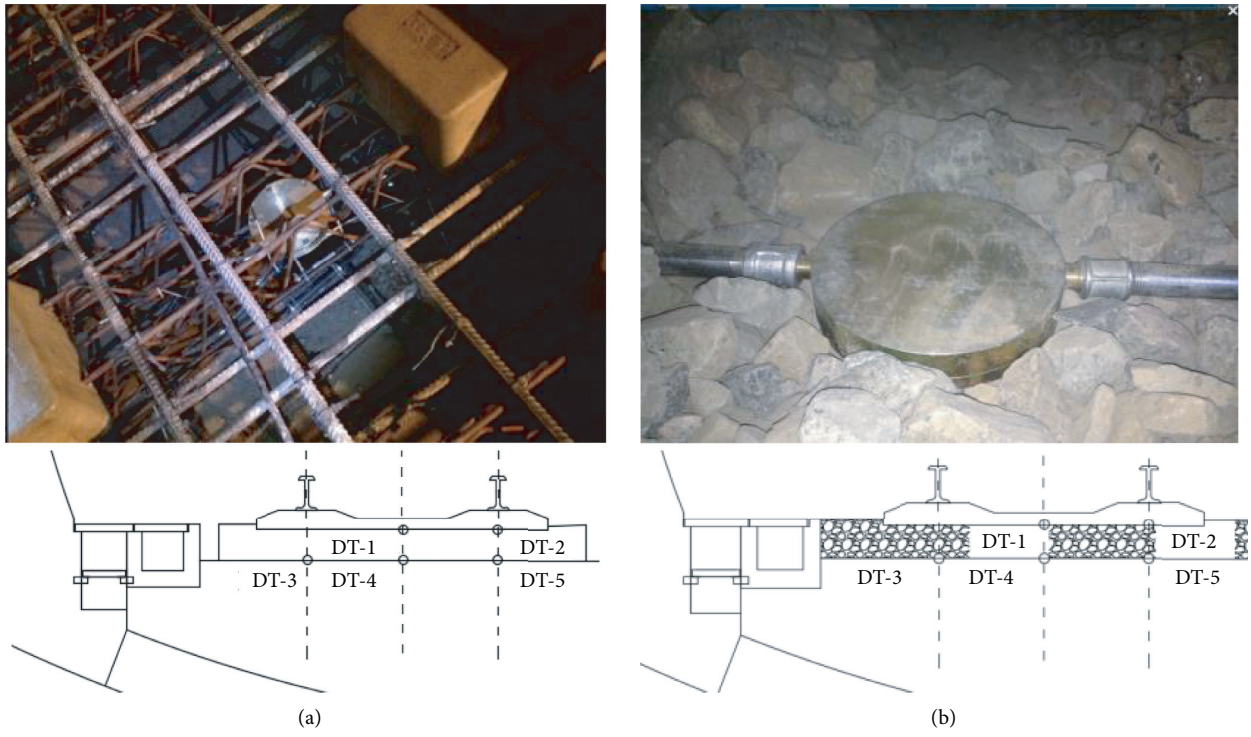

Figure 3: Schematic diagram of the sensor arrangements under different track bed types. (a) Ballast slab track. (b) Ballast bed.

measuring points can be obtained; the specific analysis is described hereinafter.

4.1. Measurements at the Sleeper Bottom. The time-history curves of the dynamic load on the ballast surface are shown in Figure 6.

Figure 6 shows that under the influence of the dynamic load action of a heavy-haul train, the dynamic load time-history curve for the sleeper bottom exhibits an obvious periodicity. The vibration period of the ballastless slab track is approximately 0.59 s, which is slightly shorter than that of the ballast bed. Because the track position of different track beds is directly affected by the dynamic action of the train,

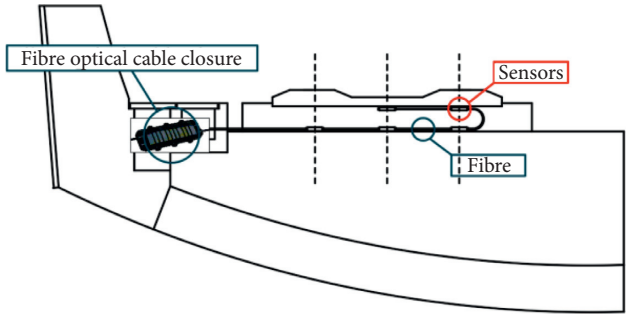

Figure 4: Schematic diagram of the sensor network.

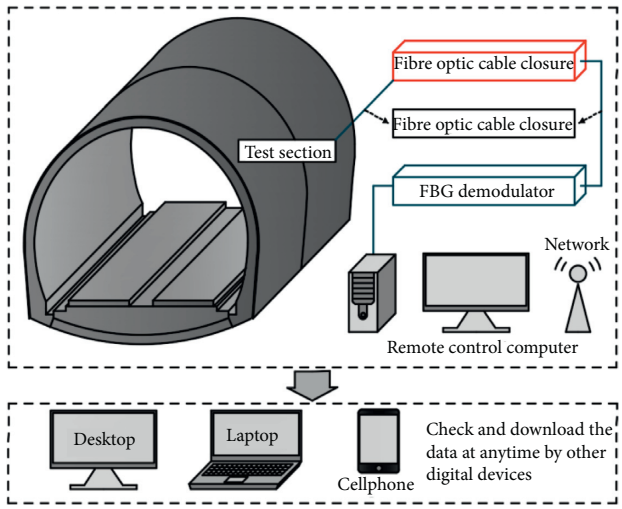

Figure 5: Remote monitoring system for the double-track heavy-haul railway tunnel.

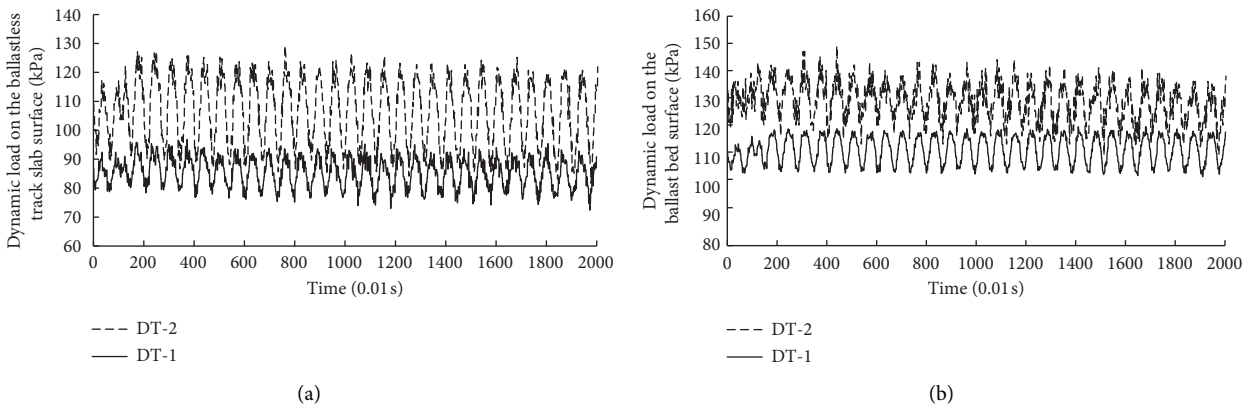

Figure 6: Typical dynamic load time-history curves for different track bed surfaces under an axis load of 270 kN. (a) Ballastless slab track surface (sleeper bottom). (b) Ballast bed surface (sleeper bottom).

the dynamic load changes more dramatically at the track position than at the central position of the transmission line. The dynamic response of the surface of the ballastless slab track is more severe than that of the ballast bed. These results indicate that the ballast can effectively buffer the dynamic effect of the train, and the ballast bed has a more obvious effect on increasing the elasticity and reducing vibrations from the heavy-haul train load than the ballastless slab track. In Table 2, the dynamic load thresholds for each measuring point on the surface of the different track beds are extracted and compared to the theoretical calculation results obtained with equation (3).

In Table 2, under the influence of the dynamic load action of heavy-haul trains, the dynamic load threshold at

Table 2: Dynamic loads at the sleeper bottom.

Track bed	Measured value (kPa)		Equation (3) (kPa)
	Line centre position	Track position	
Ballastless slab track	98.850	126.700	139.696
Ballast bed	119.402	145.278	

the track position in the ballast bed reaches 145.278 kPa, which is approximately 14.7% higher than the 126.700 kPa in the ballastless slab track. On the other hand, the dynamic load threshold at the line centre in the ballastless slab track is 98.850 kPa, accounting for 78.02% of the track position, while the centre of the ballast bed accounts for 82.19% of the track position. These results show that the cushioning property of the ballast bed is better than that of the ballastless slab track, and the ballast bed creates more uniform stress on the sleeper bottom; it also bears a greater load action from heavy-haul trains. Both the ballast bed and ballastless slab track are symmetrical structures, and it can be concluded that under the influence of the dynamic load action of heavy-haul trains, the dynamic load distribution on the sleeper bottom with the different track beds is "saddle-shaped"; i.e., the dynamic load value is at a maximum below the track and decreases towards the track centre and ends. The details are shown in Figure 7.

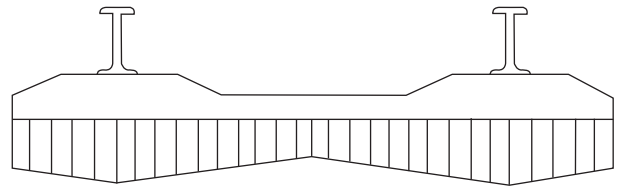

Figure 7: Dynamic load distribution on the sleeper bottom under different track beds.

Equation (3) is used to calculate the train dynamic load on the sleeper bottom. Comparing the theoretical results with the measured values at the track position of different types of track bed, the error of the ballastless slab track bed is 9.30%, while that of the ballast bed is 4.00%. This demonstrates that the measured results agree well with the theoretical results obtained with equation (3). Thus, the dynamic load threshold of the sleeper bottom with different ballast types in heavy-haul railway tunnels can be estimated using equation (3).

4.2. Measurement at the Filling Layer Surface. The time-history curves of the dynamic load from the train on the ballast bottom (filling layer surface) of the Fuyingzi Tunnel and Hongshila Tunnel are shown in Figure 8; because the measuring points are symmetrically distributed, only the DT-4 and DT-5 time-history curves are shown.

In Figure 8, under the influence of the dynamic load action of heavy-haul trains, the dynamic load time-history curve of the ballast bottom (filling layer surface) is also periodic. The vibration period of the ballastless slab track is approximately 0.65 s, and the vibration period of the ballast bed is 0.78 s, which is greater than that of the ballastless slab track. The distributions of the dynamic load threshold at the ballast bottom differ for the two types of track bed. The dynamic load at the centre of the ballastless slab track is larger than that in other positions; however, the dynamic load at the track position of the ballast bed is larger than that at the line centre position. The dynamic response of the contact pressure on the ballastless slab track bottom is more severe than that of the ballast bed, which indicates that the ballast still plays an active role in reducing the dynamic vibration when the train load is transferred to the filling layer surface. The dynamic load thresholds at each measuring point on the surfaces of different track beds are extracted and compared with the theoretical results obtained with equation (3) in Table 3.

In Table 3, under the influence of the dynamic load action of heavy-haul trains, the threshold of the train dynamic load on the filling layer surface of the ballastless slab track reaches 62.947 kPa, which appears in the line centre and is attenuated by 50.32% compared to the surface. The threshold of the train dynamic load on the filling layer surface of the ballast bed reaches 103.496 kPa, which appears in the track position and is attenuated by 29.96% compared to the surface. The dynamic load threshold at the track position of the ballastless slab track is 46.664 kPa, which accounts for 72.54% of the line centre position; however, in the ballast bed, the line centre position accounts for 75.27% of the track position. In summary, compared to the ballast bed, the ballastless slab track is more conducive to heavy-haul train load diffusion and load bearing in the filling layer.

The distribution of the dynamic load on the ballast bottom exhibits clear differences between the ballast bed and the ballastless slab track slab. The ballastless slab track manifests as a "triangular" distribution, in which the load is at a maximum at the line centre and gradually decreases towards both ends. In the case of the ballast bed, the load is greatest at the left and right rails, followed by the central position of the line; i.e., the load distribution form is similar to the "saddle-shaped" distribution. The specific load distributions are shown in Figure 9.

In Figure 9, during the vertical load transfer of a heavy-haul train, the stress diffusion angle of the ballastless slab track is larger than that of the ballast bed. Therefore, owing to the stress superposition, the dynamic load at the line centre position on the filling layer surface of the track bed in the ballastless slab track is clearly higher than that on both sides. In contrast, because the stress diffusion angle of the ballast bed is small, the dynamic loads on its filling layer surface mainly concentrate in the left and right track positions, which is consistent with the distribution on the ballast bed surface.

Equation (3) is used to calculate the dynamic load threshold on the ballast bed bottom (i.e., the filling layer

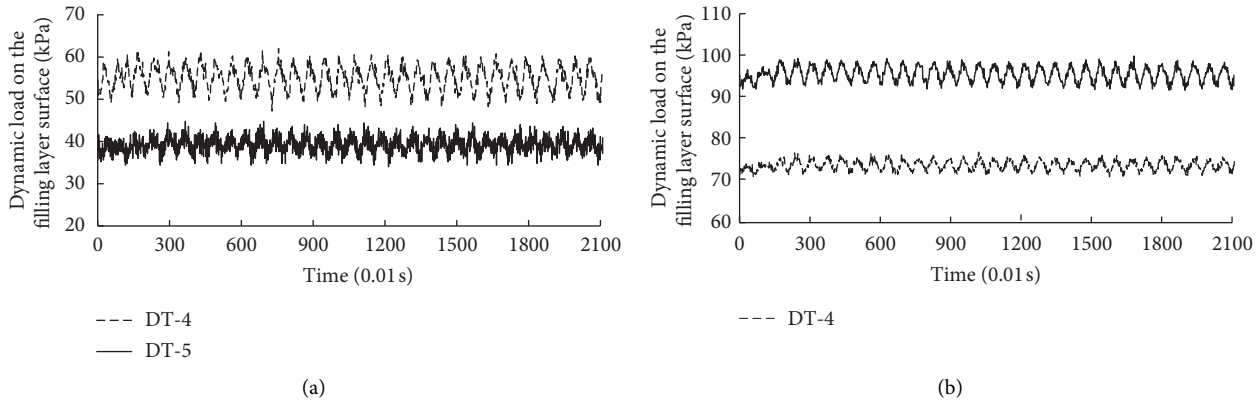

Figure 8: Typical dynamic load time-history curves for different track bed bottoms under a 270 kN axis load. (a) Ballastless slab track bottom (filling layer surface). (b) Ballast bed bottom (filling layer surface).

Table 3: Dynamic loads on the sleeper bottom.

Track bed	Measured value (kPa)			Equation (3) (kPa)
	Left side track	Line centre position	Right side track	
Ballastless slab track	43.856	62.947	45.664	69.848
Ballast bed	103.496	76.588	101.750	99.753

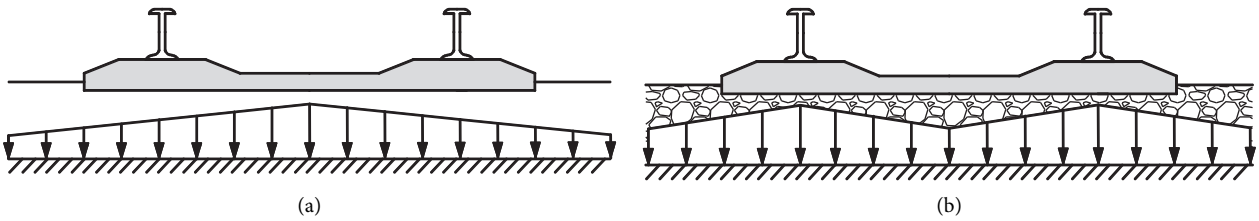

Figure 9: Distribution of the dynamic loads at the sleeper bottom with different track beds. (a) Load distribution at the ballastless slab track bottom. (b) Load distribution at the ballast bed bottom.

surface), and the theoretical calculation results are compared to the measured values at the bottom of the different track beds. The error of the ballastless slab track is 9.88%, and the error of the ballast bed is 2.00%, which indicates that the measured results are in good agreement with the theoretical calculation values from equation (3). Therefore, the train dynamic load threshold at the bottom of different track beds (filling layer surface) of heavy-haul railway tunnels can be estimated using equation (3).

4.3. Verification of Class IV and V Surrounding Rocks. In the above analysis of the characteristics of the ballast bed and ballastless slab track under the condition of class III surrounding rock, it is clear that theoretical equations (2) and (3) have a higher consistency for calculating the dynamic load threshold of the ballast bed than that of the ballastless track slab. In addition, the ratio of the dynamic load threshold in the line centre position to that in the track position is 0.78–0.82, and this ratio is used as the attenuation coefficient to fit the transverse distance between the measured point and the track position to obtain the attenuation curve. Finally, equation (2) is modified to obtain equation (4)

$$\sigma = [1 - 0.3x \cdot \mathrm{Sgn}(x)] \cdot \frac{\gamma P \cdot (1 + \alpha v)}{\mathrm{BL}}, \tag{4}$$

where x is the transverse distance between the measuring point and the track position, for which the track position of the heavy-haul line is taken as 0 m, the centre position of the heavy-haul line is taken as 0.7 m, and x does not exceed half the value of the line centre (0.7 m); the remaining symbols are the same as above. In addition, Sgn (x) is a symbolic function: if $x > 0$, then Sgn $(x) = 1$; and if $x < 0$, then Sgn $(x) = -1$.

Based on the same idea, the calculation method for the dynamic load on the bottom of different track beds can be obtained. The ballastless slab track is calculated using equation (5), and the ballast bed is calculated using equation (6).

$$\sigma_h = (0.4x + 0.72) \cdot \frac{\gamma \cdot P(1 + \alpha v)}{2\mathrm{BL} \cdot \tan \varphi}, \quad (5)$$

$$\sigma_h = (-0.36x + 1) \cdot \frac{\gamma \cdot P(1 + \alpha v)}{2\mathrm{BL} \cdot \tan \varphi}. \quad (6)$$

The symbols in these equations are as described above.

In this section, the mechanical characteristics of the ballastless slab track and the applicability of theoretical equations (5) and (6) under class IV and V surrounding rock conditions in the Fuyingzi Tunnel are further analysed.

4.3.1. Track Bed Surface. According to the method described in Section 3.1, the dynamic loads on the track bed surface (sleeper bottom) under different surrounding rock conditions are extracted and listed in Table 4; these results are then compared to the measured results and the theoretical calculations under the class III surrounding rock. The transverse distribution law is shown in Figure 10.

The results in Table 4 indicate that the worse the surrounding rock condition is, the higher the dynamic load on the track bed surface will be. The growth rate of the dynamic load at the track position is greater than that at the line centre; it reaches 6.22% when class III surrounding rock is changed to class IV, and 2.29% when class IV surrounding rock is changed to class V. However, the increase is small. These results show that the dynamic load on the track bed surface is slightly affected by the surrounding rock.

In addition, the growth rate of the dynamic load at the filling layer surface under different surrounding rock conditions is higher than that at the ballast surface, which indicates that the contact pressure between the tunnel basement structure layers is gradually enhanced from top to bottom by the influence of the surrounding rock grade.

In Figure 10, the dynamic loads on track bed surface all show that the value at the line centre position is higher than at the track position under different surrounding rock conditions. The "saddle-shaped" lateral load distribution on the track bed surface is universal for the ballastless slab track. The error between the measured and theoretical dynamic loads at the ballastless slab track surface under class III surrounding rock is 9.3%–10.4%; the error is 6.5%–9.0% under class IV surrounding rock and 2.7%–6.1% under class V surrounding rock. These results show that equation (5) can be used to estimate the dynamic load on the track bed surface of the ballastless slab track.

4.3.2. Track Bed Bottom. The dynamic loads at the track bed bottom (filling layer surface) under different surrounding rock conditions are extracted and listed in Table 5 and then compared to the measured results and theoretical calculation results from equation (6) under the class III surrounding rock. The transverse distribution law is shown in Figure 11.

In Table 5, the variation in the dynamic load on the ballast bed bottom indicates that the worse the surrounding rock condition, the higher the dynamic load will be. The growth rate of the dynamic load at the track position of the ballast bed bottom is larger than that at the line centre; it reaches 7.71% when class III surrounding rock is changed to class IV and 12.46% when class IV surrounding rock is changed to class V. Furthermore, the dynamic load growth rate of track bed bottom is higher than that of the track bed surface. These results show that the influence of the surrounding rock on the contact pressure between layers of the tunnel basement structure increases gradually from top to bottom.

In Figure 11, the dynamic loads at the track bed bottom all show that the value at the line centre position is higher than that at the track position under different surrounding rock conditions. A "triangular" lateral load distribution at the track bed surface is universal for the ballastless slab track. The error between the measured and theoretical dynamic loads at the ballastless slab track bottom under class III surrounding rock is 10.1%–11.0%; the error is 2.2%–12.7% under class IV surrounding rock and 3.4%–7.7% under class V surrounding rock. These results show that equation (6) can be used to estimate the dynamic load at the track bed bottom of the ballastless slab track.

5. Analysis of Long-Term Effect

The mechanical characteristics of different track bed types under the influence of the dynamic load action of heavy-haul trains, as well as the accuracy and applicability of theoretical equations (3) and (5), were analysed and verified in the previous section. This section presents an analysis of the long-term effect of different track bed types under class III surrounding rock conditions. Based on the test results of the dynamic data, only the maximum dynamic train load measurement points on the surface and bottom of the track bed are considered.

5.1. Long-Term Effect on the Track Bed Surface. The maximum dynamic load appears in the track position at the surface of different track bed types. The tunnel structure is statically indeterminate and the structural stress caused by the long-term load is difficult to release. Thus, for convenience of the comparative analysis, the long-term dynamic pressure change at the track position of different track bed types is shown in Figure 12, starting with the data recorded on the first day of operation.

In Figure 12, with increasing time, the dynamic pressure at the track position on the surface of the different track bed types increases continuously. The dynamic pressure of the ballast bed increases more than that of the ballastless track slab, but the change is relatively stable. The dynamic pressure of the ballast bed tends to be stable at day 223, and the maximum increase is 95.389 kPa; the dynamic pressure of the ballastless slab track tends to be stable at day 166, and the maximum increase is 64.362 kPa.

5.2. Long-Term Effect on the Track Bed Bottom (Filling Layer Surface). The maximum dynamic load at the track bed bottom of the ballastless slab track appears in the line centre position, while that of the ballast bed appears at the track

Table 4: Dynamic load on the track bed surface of the ballastless slab track under different surrounding rock conditions (kPa).

Location		Class III	Growth rate	Class IV	Growth rate	Class V	Theoretical value
Track bed	Line centre	98.850	6.22	105.000	2.29	107.400	110.360
Surface	Track	126.700	3.08	130.600	0.46	131.200	139.696

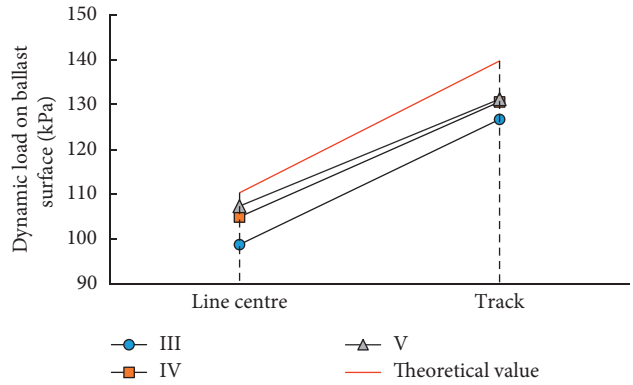

Figure 10: Distribution of the dynamic load on the track bed surface of the ballastless slab track.

Table 5: Dynamic load on the track bed bottom of the ballastless slab track under different surrounding rock conditions (kPa).

Location		Class III	Growth rate	Class IV	Growth rate (%)	Class V	Theoretical value
Track bed surface	Left side track	43.856	7.17	47.000	12.46	52.857	50.327
	Line centre	62.947	3.58	65.200	10.85	72.272	69.848
	Right side track	45.664	2.49	46.800	16.43	54.489	50.327

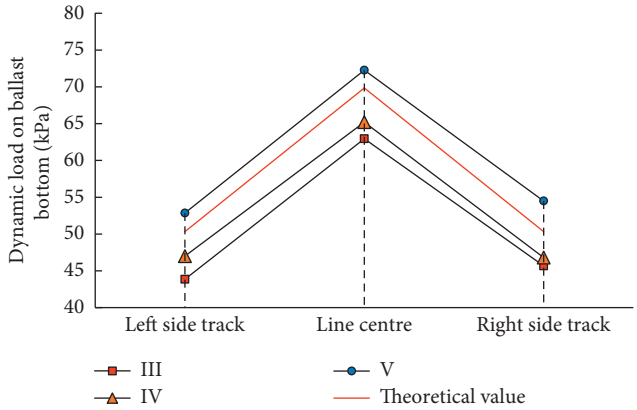

Figure 11: Distribution of the dynamic load on the track bed bottom of the ballastless slab track.

position. Therefore, the long-term dynamic pressure changes at these two points are compared in Figure 13.

In Figure 13, the dynamic pressure at the surface of different track bed types still increases with time, and the amount of increase is clearly less than that recorded at the track bed surface. The dynamic pressure of the ballast bed exhibits a steady increase and the maximum increment is greater than that of the ballastless track slab. Specifically, the dynamic pressure of the ballast bed tends to be stable around day 220, and the maximum increase is 70.495 kPa. The dynamic pressure at the surface of the ballastless slab track changes relatively violently, but the maximum increase is small; it tends to be stable around day 114, and the maximum increase is 45.384 kPa.

According to this comprehensive analysis, the long-term effect of the dynamic pressure on the surface of different track bed types is more significant than that on the bottom under the same surrounding rock conditions and driving parameters. The dynamic pressure of the ballast bed increases slowly, but the overall increase is larger, while the

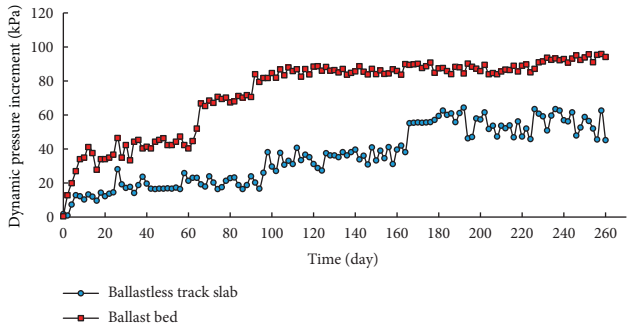

Figure 12: Long-term effect of the dynamic pressure on the track bed surface.

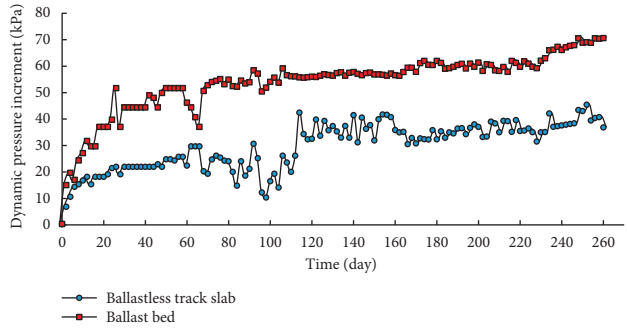

Figure 13: Long-term effect of the dynamic pressure at the track position on the track bed bottom.

dynamic pressure of the ballastless slab track changes relatively violently over a long period of time, but the overall increase is smaller. The reason for this phenomenon is that the ballastless slab track has good integrity, but its cushioning property is poor, and most of the dynamic loads caused by heavy-haul trains are diffused during the service period of the ballastless track slab. Because the ballast bed is composed of a ballast that experiences a gradual decrease in density and elasticity, the dynamic pressure exhibits a steady growth under the long-term influence of the dynamic load action of heavy-haul trains during the service period of the ballast bed.

6. Conclusions

Based on the mechanical characteristics of two types of track beds and the wheel-rail sharing ratio, calculation methods for the dynamic loads on the surface and bottom of ballastless slab tracks and ballast beds in heavy-haul railway tunnels are proposed. In addition, the dynamic load distribution of the different track bed types is analysed based on field monitoring of the Zhangtang Railway, and the theoretical calculation method is verified. The main conclusions are as follows:

(1) The pseudo-static method can be used to estimate the dynamic load on the surface of different types of track beds in terms of the axle load, train speed, force bearing area of the sleeper bottom, and wheel-rail sharing ratio of heavy-haul trains. In addition, introducing the wheel-rail sharing ratio into the theoretical stress diffusion angle can be used to estimate the dynamic loads on the bottom of different track bed types, significantly simplifying the calculation method under the influence of the dynamic load action of heavy-haul trains

(2) Under the same surrounding rock conditions and heavy-haul trainload, the vibration period of the ballast bed and ballastless slab track increases with increasing vertical depth. Moreover, the vibration period of the ballastless slab track is shorter than that of the ballast bed. This indicates that the ballast can buffer the dynamic load of heavy-haul trains, and the ballast bed has better elasticity and vibration reduction. However, the ballast bed will bear a greater dynamic load, and the dynamic load on the bottom of the ballast bed is increased by approximately 14.7% compared to the ballastless slab track

(3) The dynamic load distributions on the surface of the two types of track bed are "saddle-shaped". When the train-induced dynamic load is transferred to the filling layer surface, the transverse distribution in the ballast bed is the same as that on the surface, while the distribution at the filling layer surface of the ballastless slab track is "triangular". In addition, the degree of attenuation of the train-induced dynamic load on the bottom of the ballastless track slab is greater than that on the ballast bed. Thus, the ballastless slab track is more conducive to the diffusion of train-induced dynamic loads and the surface bearing capacity of the filling layer

(4) The surrounding rock condition has little effect on dynamic load on the surface of the ballastless slab track, and the influence of the surrounding rock condition increases with increasing vertical depth. Under different surrounding rock conditions, the dynamic load distributions on the surface and bottom of the ballastless slab track are consistent. The threshold values are in good agreement with those calculated using equations (5) and (6), which reflects the applicability of the theoretical equations

(5) The dynamic long-term effect on the two types of track bed gradually decreases from top to bottom under the same conditions. The dynamic pressure of the ballast bed increases slowly, but the overall increase is larger. However, the maximum increase in the ballastless slab track is relatively small, but the dynamic long-term effect on the ballastless slab track is more intense than that on the ballast bed. Furthermore, the time to reach a stable dynamic pressure increase on the surface and bottom of the ballastless slab track is less than that of the ballast bed.

Data Availability

The data used to support the findings of this study are available from the corresponding author upon request.

Conflicts of Interest

The authors declare that they have no conflicts of interest.

Acknowledgments

The authors would like to acknowledge the constructive comments and suggestions made by the Open-End Fund of Key Laboratory of New Technology for Construction of Cities in Mountain Area (LNTCCMA-20210108), the National Natural Science Foundation of China (5108098, 51508475, and 51878568), the Chongqing Education Commission Science and Technology Research Project (KJQN201901509), the Sichuan University Key Laboratory Foundation of Bridge Nondestructive Testing and Engineering Calculation (2018QYJ06), the Chongqing University of Science and Technology Graduate Innovation Program Project (YKJCX2020664), the Chongqing Natural Science Fund General Project (cstc2020jcyj-msxmX0904), and the Chongqing Talent Plan (CQYC2020058263).

References

[1] Z.-X. Geng, X.-F. Li, and B. Zhang, "Simulation study of heavy haul train operation on datong-qinhuangdao railway," *China Railway Science*, vol. 29, no. 2, pp. 88–93, 2008.

[2] Y. Davydov, T. Kalikina, and A. Plyaskin, "The heavy haul train service on the eastern section of the baikal-amur mainline," *Procedia Engineering*, vol. 187, pp. 769–774, 2017.

[3] L. A. Carrascal, J. A. Casado, and F. Gutierrez-Solana, "Dynamic behaviour of railway fastening setting pads," *Journal of Engineering Failure Analysis*, vol. 14, no. 26, pp. 364–373, 2007.

[4] J. Bian, Y. T. Gu, and M. Murray, "Numerical study of impact forces on railway sleepers under wheel flat," *Advances in Structural Engineering*, vol. 16, no. 1, pp. 127–134, 2013.

[5] Z. Li, Z. Li, R. Cai et al., "Dynamic pressure response of foundation base structure in heavy haul railway tunnel," *China Railway Science*, vol. 37, no. 1, pp. 71–78, 2016.

[6] S. Bressi, G. D'Angelo, J. Santos et al., "Environmental performance analysis of bitumen stabilized ballast for railway track-bed using life-cycle assessment," *Construction and Building Materials*, vol. 188, pp. 1050–1064, 2018.

[7] F. Lamas-Lopez, J. Yu, S. NicolasCalon et al., "Track-bed mechanical behaviour under the impact of train at different speeds," *Soils and Foundations*, vol. 56, no. 4, pp. 627–639, 2016.

[8] C. Ganzalez-Nicieza, M. I. Alvarez-Fernandez, and A. Menendez-Diaz, "Failure analysis of concrete sleepers in heavy haul railway tracks," *Engineering Failure Analysis*, vol. 15, no. 1-2, pp. 90–117, 2008.

[9] L. A. Yang, W. Powrie, and J. A. Priest, "Dynamic stress analysis of a ballasted railway track bed during train passage," *Journal of Geotechnical & Geoenvironmental Engineering*, vol. 135, no. 5, pp. 680–689, 2009.

[10] J. Sadeghi, "Field investigation on dynamics of railway track Pre-stressed concrete sleepers," *Advances in Structural Engineering*, vol. 13, no. 1, pp. 139–151, 2010.

[11] G. Lazorenko, A. Kasprzhitskii, Z. Khakiev et al., "Dynamic behavior and stability of soil foundation in heavy haul railway tracks: a review," *Construction and Building Materials*, vol. 205, pp. 111–136, 2019.

[12] P. Xu and C. Cai, "Spatial dynamic model of train-ballast track-subgrade coupled system," *Engineering Mechanics*, vol. 28, no. 3, pp. 191–197, 2011.

[13] X. Yang, L. Gao, G. Yang et al., "Fine modelling of ballast grains and influence on mechanical properties of track bed," *Journal of the China Railway Society*, vol. 36, no. 9, pp. 73–78, 2014.

[14] A. Namura, Y. Kohata, and S. Niura, "Study on the optimum size of railway sleeper for ballasted track," *Journal of Structural and Earthquake Engineering*, vol. 22, no. 2, pp. 245–255, 2005.

[15] J. Sadeghi, "Experimental evaluation of accuracy of current practices in analysis and design of railway track sleepers," *Canadian Journal of Civil Engineers*, vol. 35, no. 9, pp. 881–893, 2008.

[16] Z. Li, M. Wang, L. Yu, and Y. Zhao, "Study of the basement structure load under the dynamic loading of heavy-haul railway tunnel," *International Journal of Pavement Engineering*, vol. 21, no. 11, pp. 1362–1373, 2020.

[17] W.-Q. Lv, "Structural analysis and design method for subgrade Bed of heavy haul railway," *Journal of the China Railway Society*, vol. 38, no. 4, pp. 74–80, 2016.

[18] China Railway Publishing House, *Code for Design on Subgraed of Railway*, China Railway Publishing House, Beijing, China, 2005.

[19] P. Sangat and M. Indrawan-Santiago, "Processing high-volume geospatial data: a case of monitoring heavy haul railway operations," *Procedia Computer Science*, vol. 80, pp. 2221–2225, 2016.